Article

Cell Reports

SART3-Dependent Accumulation of Incomplete Spliceosomal snRNPs in Cajal Bodies

Graphical Abstract

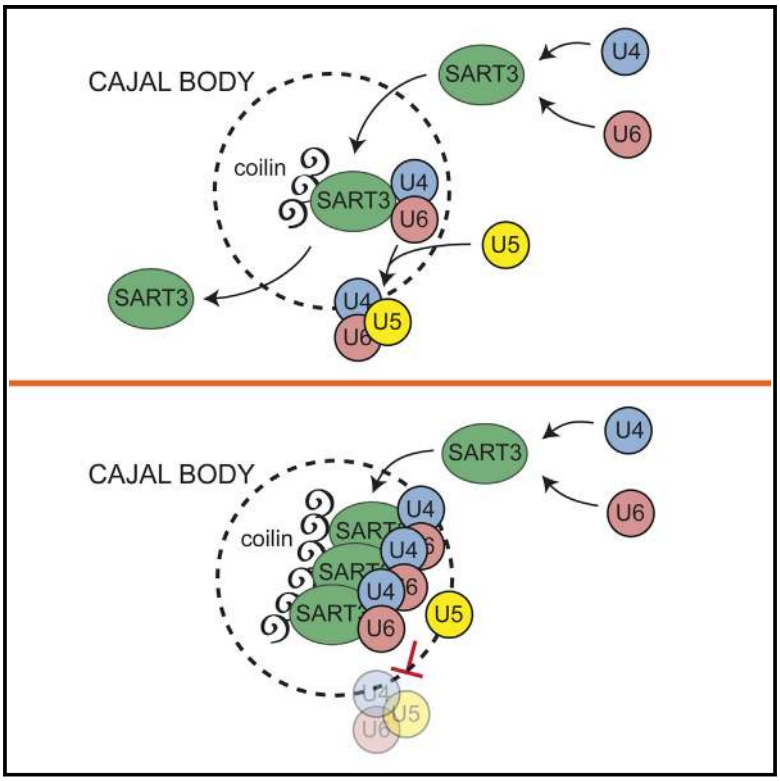

Highlights

- Inhibition of snRNP assembly induces new Cajal bodies
- Stalled snRNP assembly intermediates accumulate in Cajal bodies
- SART3 interacts with coilin and anchors incomplete snRNPs to Cajal bodies
- SART3 and Cajal bodies survey snRNP assembly

Authors

Ivan Novotný, Anna Malinová, ..., Zdeněk Knejzlík, David Staněk

Correspondence

david.stanek@img.cas.cz

In Brief

Cajal bodies are nonubiquitous nuclear structures involved in snRNP biogenesis. Novotný et al. demonstrate that Cajal body formation is triggered by inhibition of snRNP assembly. Stalled assembly intermediates highly accumulate in these bodies, which indicate that Cajal bodies are involved in quality control of snRNP assembly.

Novotný et al., 2015, Cell Reports *10*, 429–440
January 20, 2015
http://dx.doi.org/10.1016/j.celrep.2014.12.030

CellPress

Cell Reports
Article

SART3-Dependent Accumulation of Incomplete Spliceosomal snRNPs in Cajal Bodies

Ivan Novotný,[1] Anna Malinová,[1] Eva Stejskalová,[1] Daniel Matějů,[1] Klára Klimešová,[1] Adriana Roithová,[1] Martin Švéda,[2] Zdeněk Knejzlík,[2] and David Staněk[1,*]
[1]Department of RNA Biology, Institute of Molecular Genetics AS CR, 142 20 Prague, Czech Republic
[2]Department of Biochemistry and Microbiology and Center of Applied Genomics, Institute of Chemical Technology, 166 28 Prague, Czech Republic
*Correspondence: david.stanek@img.cas.cz
http://dx.doi.org/10.1016/j.celrep.2014.12.030

SUMMARY

Cajal bodies (CBs) are evolutionarily conserved nuclear structures involved in the metabolism of spliceosomal small nuclear ribonucleoprotein particles (snRNPs). CBs are not present in all cell types, and the trigger for their formation is not yet known. Here, we depleted cells of factors required for the final steps of snRNP assembly and assayed for the presence of stalled intermediates in CBs. We show that depletion induces formation of CBs in cells that normally lack these nuclear compartments, suggesting that CB nucleation is triggered by an imbalance in snRNP assembly. Accumulation of stalled intermediates in CBs depends on the di-snRNP assembly factor SART3. SART3 is required for both the induction of CB formation as well as the tethering of incomplete snRNPs to coilin, the CB scaffolding protein. We propose a model wherein SART3 monitors tri-snRNP assembly and sequesters incomplete particles in CBs, thereby allowing cells to maintain a homeostatic balance of mature snRNPs in the nucleoplasm.

INTRODUCTION

Spliceosomal small nuclear ribonucleoprotein particles (snRNPs) are key components of the splicing machinery. Five major snRNPs have been identified and named according to the RNA subunit they contain: U1, U2, U4, U5, and U6. All of these small nuclear RNAs (snRNAs) (except U6) are transcribed by RNA polymerase II and leave the cell nucleus shortly after synthesis. Once in the cytoplasm, the 5′ end is hypermethylated to produce a trimethylguanosine cap and the SMN complex assembles a ring of seven Sm proteins on the snRNA to form a core snRNP. The core snRNP is then reimported to the nucleus, where it first appears in the nuclear structure named the Cajal body (CB) (Sleeman and Lamond, 1999). In the CB, snRNAs are modified by small Cajal body-specific RNA-targeted ribose methylation and pseudouridinylation (Darzacq et al., 2002; Jády et al., 2003) and proteins specific for each snRNP are added to produce a mature snRNP (reviewed in Matera and Shpargel, 2006; Matera and Wang, 2014; Stanek and Neugebauer, 2006).

Initial steps of snRNP formation are under strict quality control. First, newly synthesized snRNAs are retained in CBs until the export complex containing the RNA export protein PHAX is properly formed (Suzuki et al., 2010). In the cytoplasm, the SMN complex ensures that Sm proteins assemble on the correct snRNA substrate (Battle et al., 2006; Chari et al., 2009). Nuclear import also serves as a quality control checkpoint in that only snRNAs with both the trimethylguanosine cap and the Sm ring are transported back to the nucleus (Marshallsay and Lührmann, 1994; Narayanan et al., 2004; Patel and Bellini, 2008). Once snRNPs are reimported to the nucleus, our understanding of their assembly and quality control becomes less clear. In fact, virtually nothing is known about surveillance of the final stages of snRNP assembly. In addition, snRNPs enter the splicing reaction repeatedly, but a molecular mechanism that controls the quality of snRNPs joining the spliceosome is elusive.

A classical example of how snRNPs form and recycle is demonstrated by the U4/U6•U5 tri-snRNP, which is (re)assembled in a stepwise process (see Figure 1A). In the first step, U4 and U6 snRNAs anneal and the U4/U6 snRNP (di-snRNP) is formed. In yeast, this step is catalyzed by Prp24p; in humans, U4/U6 snRNP assembly is promoted by the joint action of SART3 (also named p110, p110^{nrb}, Tip110, or hPrp24) and LSm2-8 proteins (Achsel et al., 1999; Bell et al., 2002; Medenbach et al., 2004; Rader and Guthrie, 2002). Next, the di-snRNP associates with the U5 snRNP, mediated through hPrp31-hPrp6 interactions (Makarov et al., 2000; Makarova et al., 2002), and the mature U4/U6•U5 tri-snRNP is formed. Human SART3 and SART3•U4/U6 snRNP complexes accumulate in CBs, indicating the U4/U6 di-snRNP assembles in this nuclear structure (Staněk and Neugebauer, 2004; Staněk et al., 2003). Addition of the U5 snRNP and tri-snRNP formation has also been localized to CBs (Schaffert et al., 2004). Once the mature tri-snRNP is fully assembled, it leaves the CB to participate in mRNA splicing. The act of splicing breaks the tri-snRNP into individual snRNPs, which are then recycled back to the CB for assembly before another round of splicing can occur (Stanek et al., 2008).

The role of CBs in snRNP metabolism is still not fully understood. In zebrafish embryos, depletion of the CB scaffolding protein coilin is lethal and can be complemented with fully

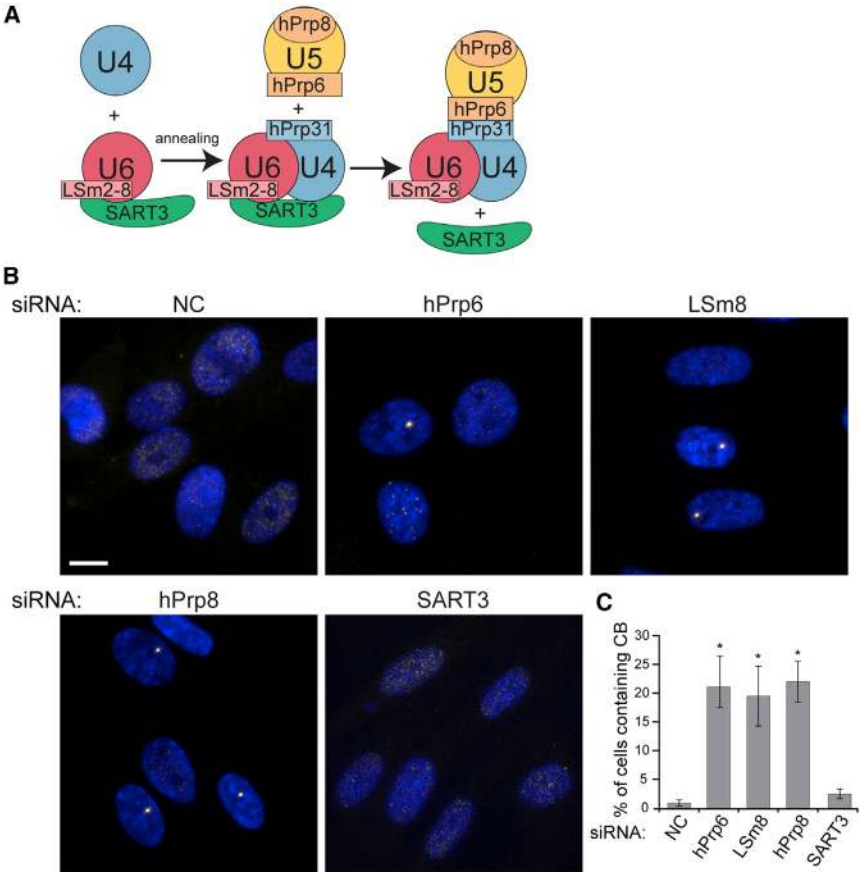

Figure 1. Inhibition of Tri-snRNP Assembly Induces New Cajal Bodies in Primary Fibroblasts

(A) A model of tri-snRNP assembly and the proteins important for individual steps.

(B) Induction of CBs by knockdown of hPrp8, hPrp6, and LSm8. CBs were visualized by immunodetection of coilin (yellow) and nuclei by DAPI staining (blue). Scale bar represents 10 μm.

(C) CBs counted by high-content microscopy. The average of three experiments is shown together with the SEM. The significance was assayed by t test against noncoding siRNA; *p ≤ 0.05.

assembled snRNPs (Strzelecka et al., 2010b), thus showing that CBs in fish embryos are essential for RNP assembly. Similarly, coilin deficiency in mice is semilethal, leading to reduced fertility and viability (Tucker et al., 2001; Walker et al., 2009). Cultured cancer cell lines depleted of coilin exhibit reduced proliferation (Lemm et al., 2006; Whittom et al., 2008), and the lack of CBs in cells derived from patients with spinal muscular atrophy correlated with reduced formation of both major and minor tri-snRNPs (Boulisfane et al., 2011). These observations are likely explained by an increase in the rate of snRNP assembly, estimated at 10-fold, due to a higher concentration of snRNP components in CBs (Klingauf et al., 2006; Novotný et al., 2011). The presence of coilin-positive CBs in a given nucleus is dependent on ongoing snRNP biogenesis, active transcription, and splicing (Ferreira et al., 1994; Lemm et al., 2006; Shpargel and Matera, 2005; Staněk et al., 2003; Strzelecka et al., 2010a). However, not all somatic cells have visible CBs, even though coilin is expressed. Thus, the endogenous trigger for CB assembly is currently unknown.

Here, we tested the importance of CBs in snRNP assembly. In cells lacking CBs, we assayed for snRNP localization after knocking down several proteins important for the final stages of tri-snRNP formation. Interestingly, these knockdowns induced formation of visible CBs that accumulated incomplete snRNPs. Similar results were observed in CB-containing cells where inhibition of tri-snRNP assembly induced accumulation of stalled snRNP assembly intermediates in CBs. Finally, we identified the di-snRNP assembly factor SART3 as the protein that tethers incomplete snRNPs to the CB scaffold protein coilin.

RESULTS

Inhibition of the Tri-snRNP Assembly Pathway Induces Cajal Body Formation in Primary Fibroblasts

Despite the well-characterized role of CBs in snRNP biogenesis, it is not clear why only some cell types contain these nuclear structures. Several lines of evidence suggest that final snRNP maturation and formation/recycling of U4/U6 and U4/U6•U5 snRNPs occur in CBs. In addition, accumulation of U4/U6 and U4/U6•U5 snRNPs in CBs increases the efficiency of their assembly (Klingauf et al., 2006; Novotný et al., 2011). We therefore tested how cells lacking CBs react to the perturbation of snRNP assembly. Utilizing human primary fibroblasts WI-38, which normally lack CBs, we knocked down several snRNP-specific proteins that were previously shown to be important for distinct steps of snRNP assembly: Prp8, which is important for U5 snRNP maturation in yeast (Boon et al., 2007); SART3 and LSm8, which are involved in U4/U6 snRNA annealing (Achsel et al., 1999; Bell et al., 2002); and hPrp6, which is essential for tri-snRNP formation (Makarov et al., 2000; Makarova et al., 2002; Schaffert et al., 2004). Depletion of three (hPrp8, LSm8, and hPrp6) out of the four tested proteins led to the formation of visible CBs (Figure 1B). To quantify the number of cells containing CBs, we utilized high-content microscopy, which allowed us to automatically collect and analyze images. CBs were detected in ~20% of the cells (Figure 1C).

To further characterize these newly formed CBs, we depleted hPrp8, LSm8, and hPrp6 and analyzed the localization of individual snRNPs and two CB proteins, SMN and fibrillarin, to CBs. While di-snRNP components accumulated in newly formed CBs in all three knockdowns (Figures 2A and 2B), we did not detect U2 snRNP components in CBs (Figure S1A). U5 snRNA accumulated in new CBs after hPrp8 and LSm8 depletion, but hSnu114, a U5-specific protein, only localized to CBs after the

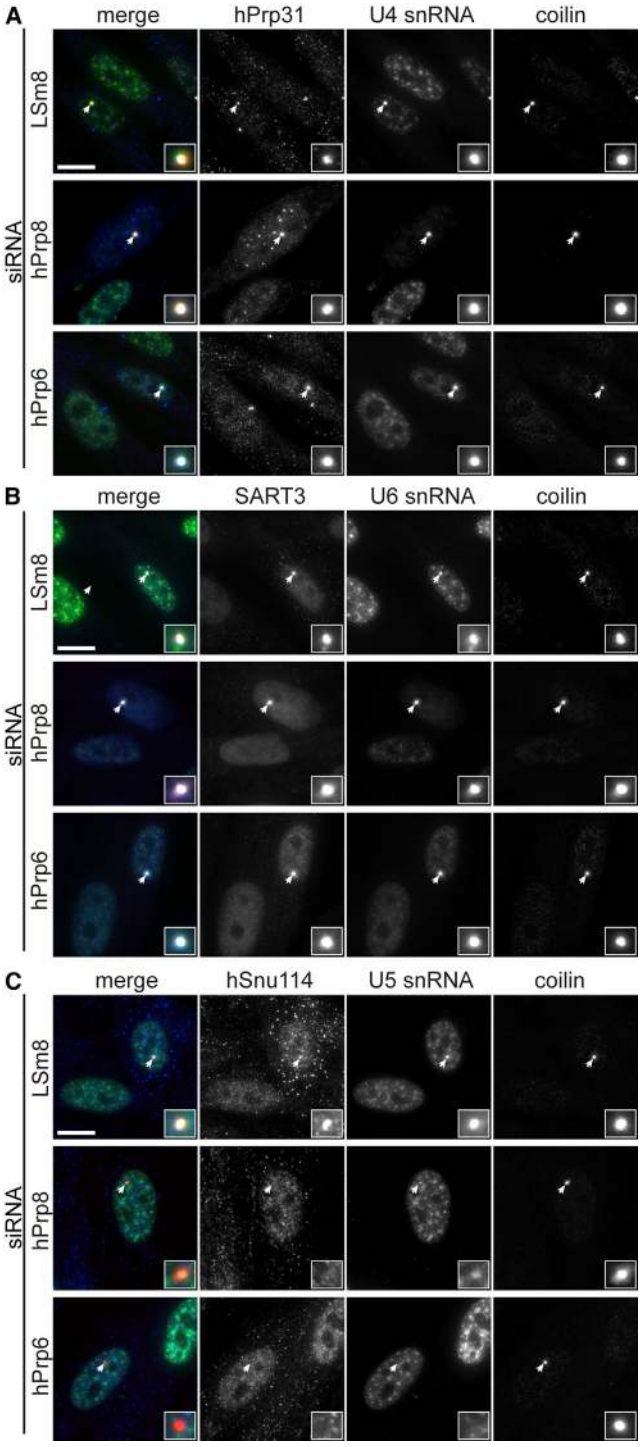

Figure 2. Newly Induced Cajal Bodies Contain U4, U5, and U6 snRNPs

(A and B) Accumulation of U4 snRNPs (A) and U6 snRNPs (B) in newly formed CBs after knockdown of hPrp8, hPrp6, or LSm8 in primary fibroblasts.

(C) U5 snRNA accumulated in CBs after LSm8 and hPrp8 knockdown.

CBs are visualized by immunodetection of coilin (red), snRNAs by in situ hybridization (green), and snRNP-specific proteins by indirect immunofluorescence (blue). CBs (marked by arrowheads) are magnified four times and shown in insets. Scale bar represents 10 μm. See also Figure S1.

downregulation of LSm8 (Figure 2C). This suggested the U5 snRNA was not associated with hSnu114 in CBs after depletion of hPrp8. In addition, we detected fibrillarin (Figure S1B), but not SMN (Figure S1C), in newly formed CBs. Instead, SMN localized to nuclear gem structures under all conditions (Figure S1C).

Stalled Tri-snRNP Assembly Intermediates Accumulate in Cajal Bodies

Next, we compared WI-38 fibroblasts with cells already containing CBs. Using human cervix carcinoma cells (HeLa), we downregulated hPrp8 and analyzed both the number of CBs and the localization of snRNAs in CBs. In contrast to primary fibroblasts, we observed no induction of new CBs (data not shown), but instead U4, U5, and U6 snRNAs accumulated in CBs (Figures 3A–3C). To test the specificity of the knockdown, we used a stable cell line expressing hPrp8-GFP from bacterial artificial chromosome (Huranová et al., 2010). The anti-hPrp8 small interfering RNA (siRNA) is designed against the sequence around the stop codon of endogenous hPrp8 and hPrp8-GFP is not targeted (Figure S6A). Expression of siRNA resistant hPrp8-GFP fully rescued the knockdown phenotype and reduced accumulation of U4, U5, and U6 snRNAs in CBs (Figures 3A–3C, bottom panel).

An increase in CB fluorescent signal could either be due to an increase in accumulated snRNAs in the CBs or to specific degradation of snRNAs in the nucleoplasm. To distinguish between these two possibilities, we measured the total nuclear signal for U4 and U6 snRNAs by high-content microscopy after hPrp8 knockdown (Figure 3D). We observed no significant decrease in the total fluorescence signal in the nucleus, indicating the apparent decrease of in situ hybridization signal in the nucleoplasm after hPrp8 knockdown was caused by redistribution of snRNAs between the nucleoplasm and CBs rather than snRNA degradation specifically in the nucleoplasm.

To obtain unbiased quantitative data about snRNP accumulation in CBs, we analyzed the nuclear distribution of snRNP components using automated high-content microscopy. By coupling microscopy with the automatic, object-based detection of CBs, we were able to calculate the fluorescence ratio between CBs and the nucleoplasm. Three independent biological experiments were performed, each containing several hundreds of cells. The high-content microscopy approach confirmed classical microscopy observations and showed that hPrp8 depletion increased accumulation of U4, U5, and U6 snRNAs in CBs. This accumulation was reversed by the expression of siRNA-resistant hPrp8-GFP (Figure 3E).

Next, we knocked down hPrp8, hPrp6, or LSm8 and monitored the accumulation of individual snRNP components in CBs by high-content microscopy (Figure 4). hPrp8 downregulation induced CB accumulation of the U4/U6-specific proteins hPrp4, hPrp31, and LSm4 (Figures 4A and 4C; see also Figures S2 and S4), while the U5-specific protein hSnu114 dropped below the level found in control cell CBs (Figures 4B and S3). Similar U4/U6 snRNP accumulation in CBs was observed after depletion of the hPrp6 protein (Figures 4A and 4C), which was previously reported by Schaffert et al. (2004). We observed identical U4/U6 snRNP accumulation in CBs using two additional siRNAs against hPrp6 (data not shown). LSm8 depletion had a pronounced effect on U4 snRNA localization and induced its

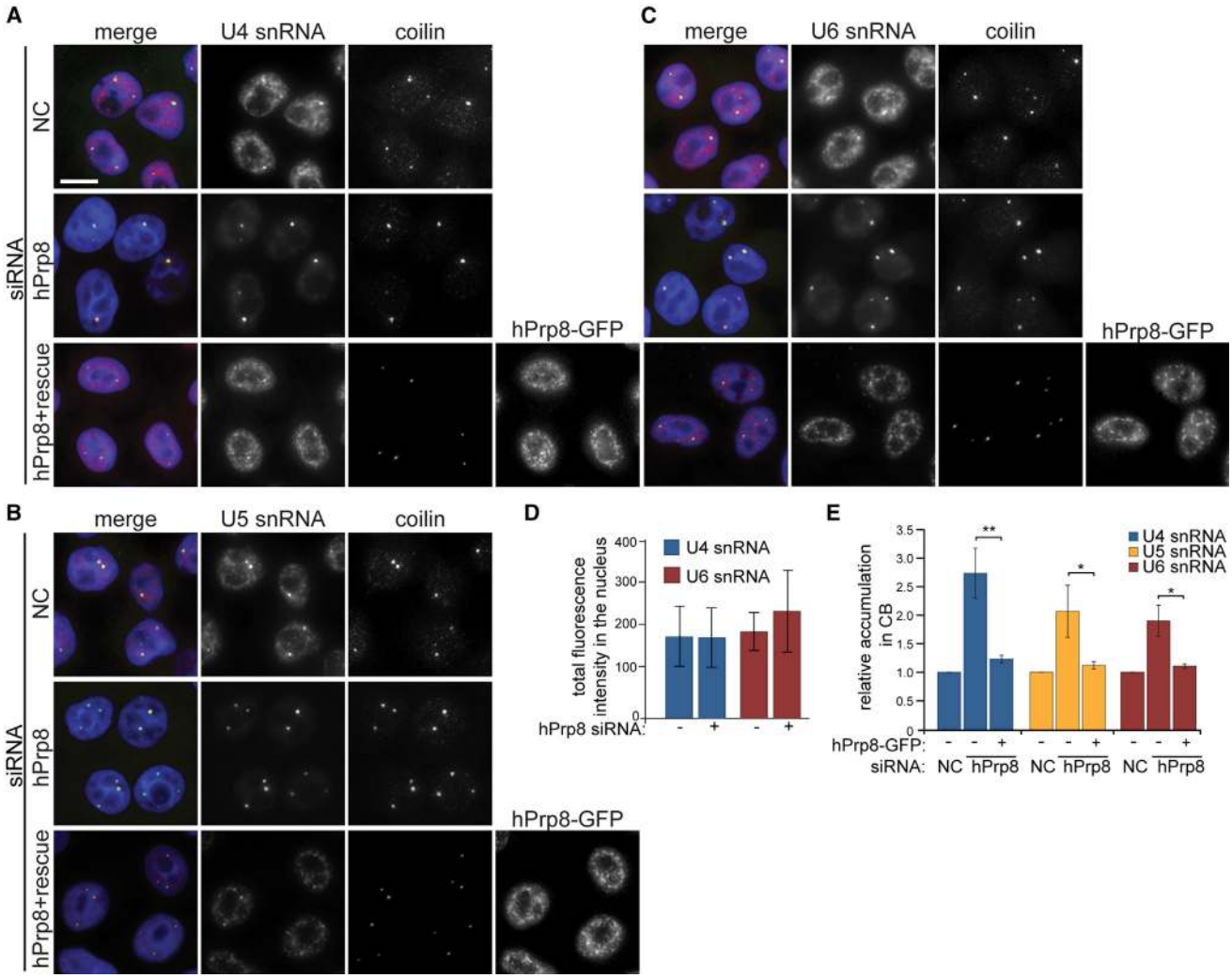

Figure 3. Depletion of hPrp8 Induces Accumulation of U4, U5, and U6 snRNAs in Cajal Bodies

(A–C) Depletion of hPrp8 induces accumulation of U4, U5, and U6 snRNAs. See also Figures S2–S4 for snRNP-specific protein localization. The normal distribution of all snRNAs was restored after expression of siRNA-resistant hPrp8-GFP. CBs were visualized by immunodetection of coilin (green) and snRNAs by in situ hybridization (red). DNA stained by DAPI (blue). Scale bar represents 10 μm.

(D) Nuclear intensities of U4 and U6 snRNAs determined by high-content microscopy followed by automated nuclear detection and measurement of fluorescence intensities inside nuclei. U4 and U6 snRNAs were detected by in situ hybridization and nuclei visualized by DAPI staining. A total of 2,300–5,300 cells were measured per experiment and the average with SD is shown.

(E) CB accumulation of snRNAs was measured by high-content microscopy. Localization of all three snRNAs in CBs was increased 2- to 3-fold upon hPrp8 knockdown and was reduced to normal levels after expression of siRNA-resistant hPrp8-GFP. The average of three experiments is shown together with the SEM. The significance was assayed by t test; *$p \leq 0.05$ and **$p \leq 0.01$.

accumulation in CBs together with the U4-specific protein hPrp31, but not the U4/U6-specific protein hPrp4 (Figure 4A). The same result was observed using two additional siRNAs against LSm8 (data not shown). As a control, we analyzed distribution of the U2 snRNP (Figure S5). Neither of the knockdowns affected CB accumulation of U2 snRNP components. In order to rule out the possibility that higher snRNP signal in CBs was due to increased accessibility of snRNP components, we utilized a cell line stably expressing the U4/U6-specific protein hPrp31 tagged with GFP (Huranová et al., 2010). hPrp31-GFP is expressed from bacterial artificial chromosome, which preserves the endogenous promoter and exon-intron structure. CB localization of hPrp31-GFP, determined directly by measuring GFP fluorescence, increased after the knockdown of all three proteins involved in snRNP assembly (Figure S6B).

These data strongly suggest that inhibition of di- and tri-snRNP assembly results in accumulation of incomplete assembly intermediates in CBs. To further test this hypothesis, we microinjected fluorescently labeled U4 snRNAs, either full-length or lacking the U6 base-pairing domain (Klingauf et al., 2006), into the cytoplasm and analyzed their accumulation in CBs over time. After the initial 30 min incubation, both snRNAs localized to CBs

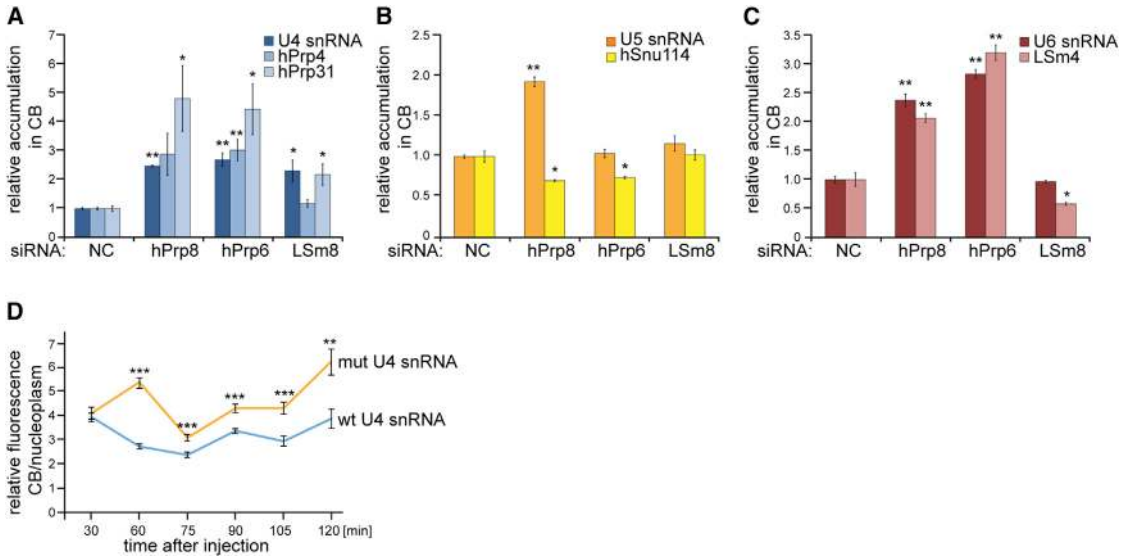

Figure 4. snRNPs Accumulate in Cajal Bodies after Inhibition of Tri-snRNP Assembly

(A–C) CB accumulation of (A) U4 snRNPs, (B) U5 snRNPs, and (C) U6 snRNPs after depletion of hPrp8, hPrp6, or LSm8 was measured by high-content microscopy. In all cases, the average of three experiments is shown together with the SEM. The significance was assayed by t test against noncoding siRNA; *$p \leq 0.05$ and **$p \leq 0.01$. See also Figures S2–S4 and S6B.

(D) Deletion of the U6-base-pairing domain from the U4 snRNA leads to higher accumulation of microinjected U4 snRNAs in CBs. Fluorescently labeled snRNAs were microinjected into the cytoplasm and incubated for the given time period and accumulation of snRNAs in CBs over nucleoplasm determined. The average of 40–80 CBs (15–25 cells) is shown together with the SEM. The significance was assayed by t test against wild-type (WT) U4 snRNA; **$p \leq 0.01$ and ***$p \leq 0.001$. See also Figure S4C.

to the same extent. However, after longer incubation periods, CB accumulation of mutant snRNA was significantly higher than wild-type snRNA (Figures 4D and S4C). These data are in agreement with our knockdown experiments and together suggest that incomplete snRNPs are sequestered in CBs.

Because hPrp4 specifically interacts with annealed U4/U6 snRNAs (Nottrott et al., 2002), lower accumulation of hPrp4 in CBs after LSm8 knockdown suggested that U4 and U6 snRNAs were not associated. This observation is consistent with previous results, which showed that LSm8 is important for the integrity of the LSm2-8 ring (Novotny et al., 2012) and that the LSm2-8 ring promotes U4/U6 snRNA annealing (Achsel et al., 1999). Reduced levels of U4/U6 snRNPs were confirmed by immunoprecipitation with U4/U6-specific proteins hPrp4 and LSm4. In both cases, we observed lower amounts of U4 and U6 snRNAs coprecipitated with these proteins after LSm8 knockdown (Figure S6C). In addition, we observed decreased amounts of the total U6 snRNA using quantitative RT-PCR, which is consistent with the role of LSm2-8 proteins in the stabilization of U6 snRNA (Figure S6D).

Downregulation of hPrp6 and hPrp8 showed a similar level of U4/U6 snRNP accumulation in CBs. hPrp6 inhibits tri-snRNP formation, and therefore this result indicates that hPrp8 knockdown prevents tri-snRNP assembly as well. To confirm this finding, we knocked down hPrp8 and analyzed formation of the mature U5 snRNP and the tri-snRNP. While hPrp8 depletion prevented association of the U5-specific proteins hSnu114, hBrr2, and hPrp6 with the core U5 snRNP (Figure 5A), it did not inhibit assembly of the Sm ring on the U5 snRNA (Figure 5B). Knockdown of hPrp8 specifically inhibited maturation of the U5 snRNP while the integrity of U4/U6 and U2 snRNPs was not affected, as indicated by coprecipitation of U2B″ and hPrp4 proteins with the Sm proteins (Figure 5A). The incomplete U5 snRNP was unable to form the tri-snRNP, as indicated by reduced coprecipitation of the U5 snRNA with U4/U6-specific hPrp4 after hPrp8 knockdown (Figure 5C). hPrp8 downregulation thus affected both the final maturation of the U5 snRNP and formation of a complete tri-snRNP.

Incomplete snRNPs Accumulate in Cajal Bodies in a SART3-Dependent Manner

Our results show that inhibition of tri-snRNP assembly at different stages results in CB accumulation of specific snRNP assembly intermediates. Our next aim was to address how incomplete snRNPs are anchored in CBs. We focused on SART3, a protein that interacts with snRNP assembly intermediates and is abundantly present in CBs where it is found in close proximity to coilin, as documented by FRET (Bell et al., 2002; Novotný et al., 2011; Staněk et al., 2003). To test whether SART3 interacts with coilin, we expressed two SART3 deletion constructs tagged with GFP and analyzed any coprecipitated snRNAs and coilin by pulling down with anti-GFP antibodies (Figure 6B). As previously shown, WT-SART3 precipitated approximately two times more U6 than U4 snRNA (Staněk and Neugebauer, 2004). The N-terminal half (ΔRRMΔCT), containing the E and tetratricopeptide repeat (TPR) domains, precipitated less overall snRNAs yet the ratio of U6:U4 shifted in favor of U4 snRNAs. This construct also precipitated a large amount of U2 snRNA. We also observed a weak coprecipitation of the U2 snRNA with WT-SART3. The amount of coprecipitated U2 snRNA correlated with the interaction of

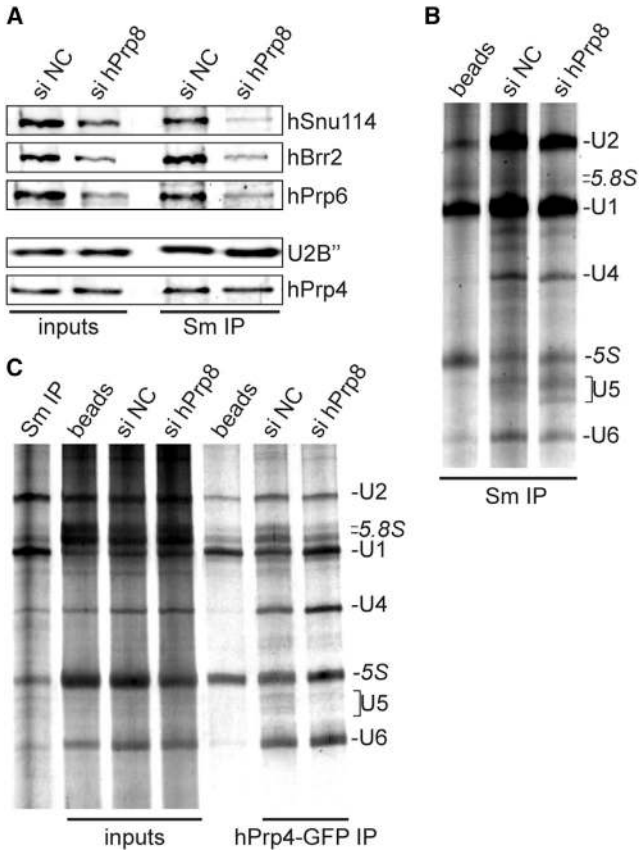

Figure 5. Downregulation of hPrp8 Inhibits U5 snRNP and Tri-snRNP Assembly

(A) hPrp8 knockdown prevents U5 snRNP formation. snRNPs were precipitated by the anti-Sm antibody, and coprecipitated snRNP-specific proteins were detected by western blotting. The amount of U5-specific proteins (hSnu114, hBrr2, and hPrp6) was significantly decreased while the amount of U4/U6 (hPrp4) and U2 snRNP-specific (U2B′′) proteins coprecipitated with Sm proteins did not change after hPrp8 knockdown.

(B) hPrp8 downregulation does not affect Sm ring formation. Sm proteins were immunoprecipitated with the anti-Sm antibody and coprecipitated snRNAs resolved on polyacrylamide gel and visualized by silver staining. Positions of individual snRNAs and rRNAs are indicated. A similar amount of U5 snRNA was coprecipitated with Sm proteins in the control and hPrp8-depleted cells.

(C) hPrp8 knockdown inhibits tri-snRNP formation. Cells stably expressing U4/U6-specific proteins hPrp4-GFP were depleted of hPrp8 and hPrp4-GFP precipitated by anti-GFP antibodies. Coprecipitated snRNAs were resolved on a polyacrylamide gel and silver stained. Positions of individual snRNAs and rRNAs are indicated. Reduced amount of the U5 snRNA was coprecipitated with hPrp4 after hPrp8 knockdown.

See also Figure S6C.

SART3 constructs with coilin (Figure 6B, bottom). The C-terminal half of SART3 (ΔEΔTPR), containing two RRMs and the C-terminal domain CT-10, mainly copurified U6 snRNA, which is consistent with previous observations (Medenbach et al., 2004; Rader and Guthrie, 2002). These results show that distinct SART3 domains interact with specific snRNPs.

Immunoprecipitation results indicated that coilin coprecipitated with SART3 and this interaction was dependent on the presence of the N-terminal domains of SART3 (Figure 6B, bottom). Coilin-SART3 interaction was confirmed by yeast two-hybrid assay, which revealed that the N-terminal E-domain of SART3 is important for this interaction (Figure 6C). We further separated the coilin sequence and showed that the N-terminal domain of SART3 interacts in a yeast two-hybrid assay with both N- and C-terminal halves of coilin, indicating two independent interaction sites within coilin (Figure S6E). Finally, we utilized structured-illumination microscopy and showed that coilin and SART3 occupied similar CB domains. In contrast, the SMN protein, which often localizes to CBs, did not colocalize with SART3 in the CB. Instead, SMN-positive structures were often found inside coilin/SART3-labeled domains and, more specifically, coilin/SART3 formed a ring-like structure around SMN (Figure 6D). Together, these data show that SART3 interacts with both snRNPs and coilin and suggest that SART3 bridges snRNP assembly intermediates and the CB scaffolding protein coilin.

To directly test whether SART3 is important for accumulation of stalled snRNP assembly intermediates in CBs, we performed several double knockdowns to deplete SART3 with hPrp6, LSm8, or hPrp8. In all cases, we observed reduced accumulation of snRNPs in CBs with respect to individual depletion of hPrp6, LSm8, or hPrp8 (Figures 7A and S2–S4). The same phenotype was observed after concomitant depletion of hPrp6 and SART3 using two different siRNAs against SART3 (data not shown). Taken together with previous results, these data showed that SART3 is an important factor in anchoring tri-snRNP assembly intermediates into CBs. Consistent with this role, SART3 pulled down more di-snRNP-specific snRNAs after inhibition of tri-snRNP assembly by hPrp6 knockdown (Figure 7B; Schaffert et al., 2004) and reduced cell proliferation when codepleted with hPrp6 (Figure 7C). Finally, we examined whether SART3 bridging between snRNPs and coilin is important for induction of CBs in primary fibroblasts. We simultaneously knocked down hPrp8 and SART3 and observed a reduced number of CBs (Figure 7D).

DISCUSSION

The CB is a multicomponent structure, which is involved in many nuclear processes. Here, we focused on the connection between CBs and snRNP biogenesis, which has been well described (reviewed in Machyna et al., 2013; Matera and Shpargel, 2006; Matera and Wang, 2014; Morris, 2008; Nizami et al., 2010; Patel and Bellini, 2008; Stanek and Neugebauer, 2006). However, it is still unclear why only some cell types contain these nuclear compartments. Here, we provide evidence that CBs are inducible structures and appear as a response to the inhibition of the snRNP assembly pathway (Figure 1). Moreover, snRNP assembly intermediates accumulate in CBs when di- and tri-snRNP formation is blocked (Figures 2, 3, and 4). We propose a model whereby the CB plays a central role in quality control of the final steps in assembly of snRNP complexes and sequesters incomplete assembly intermediates. The model is based on the following observations: (1) in cells normally lacking CBs, inhibition of tri-snRNP assembly triggers formation of CBs, which specifically accumulate incomplete snRNPs (Figures 1 and 2); (2) inhibiting different stages of tri-snRNP assembly results in the accumulation of tri-snRNP and di-snRNP assembly

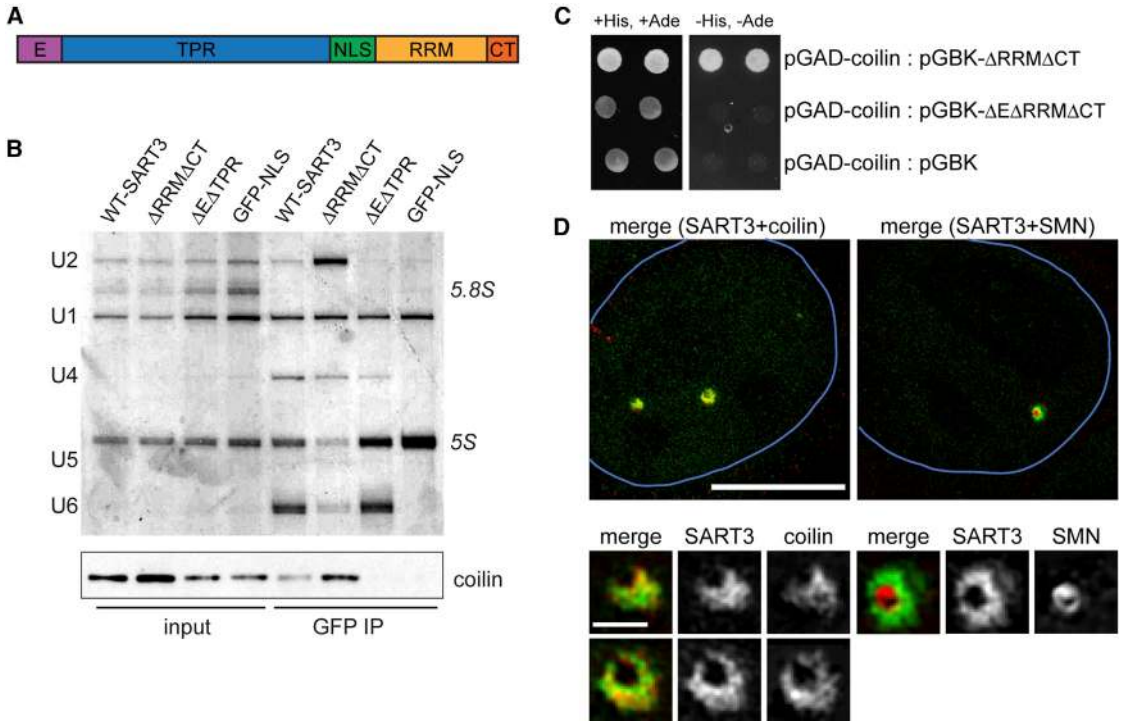

Figure 6. SART3 Interacts with Coilin

(A) A schematic representation of SART3 domain organization.

(B) Cells were transfected with different SART3 deletion constructs tagged with GFP. The SART3 constructs were immunoprecipitated by anti-GFP antibodies, and coprecipitated snRNAs were resolved on a polyacrylamide gel and silver stained. Positions of individual snRNAs and rRNAs are indicated (upper panel). Coprecipitated coilin was detected by western blotting (bottom panel).

(C) Two-hybrid assay shows interaction of the N-terminal E domain of SART3 with coilin (left panel, permissive medium; right panel, selection medium). See also Figure S6E.

(D) Structured-illumination microscopy image of SART3 with coilin or SMN in CBs. Scale bars represent 0.5 μm (insets) and 5 μm (whole nucleus). Blue line marks the nuclear edge.

intermediates in CBs (Figures 2, 3, and 4; Schaffert et al., 2004); (3) truncated U4 snRNA, which is unable to base pair with U6 snRNA, concentrates in CBs to a higher extent than wild-type U4 snRNA (Figure 4) and (Klingauf et al., 2006); and (4) immature U5 (Figures 3 and 4) and U2 snRNPs (Nesic et al., 2004; Ospina et al., 2005) accumulate in CBs.

Though the molecular mechanism of incomplete snRNP detection is unknown, here we identified SART3 as an important player in this process. SART3 interacts with the CB scaffolding protein coilin and U4, U6, and U4/U6 snRNPs and is important in the sequestration of incomplete snRNPs in CBs (Figures 6 and 7). SART3 is perfectly positioned for tri-snRNP assembly surveillance due to its interactions with the U6, U4, and U4/U6 snRNPs and its detachment as the complete U4/U6•U5 tri-snRNP is formed (Bell et al., 2002), removing the anchor and allowing the mature tri-snRNP to leave the CB. SART3 is also essential for de novo formation of CBs in primary fibroblasts triggered by stalled assembly intermediates, which is consistent with the central role of SART3 in connecting coilin and snRNPs (Figure 7D).

It was previously suggested that accumulation of U4, U5, and U6 snRNPs in CBs increased di- and tri-snRNP assembly rates ten times (Klingauf et al., 2006; Novotný et al., 2011). Therefore, concentrating assembly intermediates in CBs enhances the assembly kinetics and could compensate for low levels of tri-snRNPs. Simultaneously, the localizing of immature snRNPs in an area of inactive splicing protects the cell against aberrant snRNPs, which could potentially interfere with mRNA processing. This hypothesis would also explain why most snRNP maturation steps are localized in the cytoplasm, nucleolus, and CBs where no splicing occurs, to ensure only fully mature snRNPs could join the splicing reaction. Consistently, codepletion of SART3 with hPrp6 reduced cell proliferation (Figure 7C). While coilin and CBs are crucial for zebrafish development (Strzelecka et al., 2010b), coilin is not essential in *Drosophila melanogaster* and *Arabidopsis thaliana* (Collier et al., 2006; Liu et al., 2009). With respect to our findings, it would be interesting to test whether coilin and CBs become essential when snRNP assembly is perturbed in these model organisms.

The molecular mechanism that governs CB formation is poorly understood. CBs often associate with genes encoding U snRNAs (Frey et al., 1999; Frey and Matera, 1995; Jacobs et al., 1999; Smith et al., 1995) and artificial immobilization of CB components to chromatin nucleated CBs (Kaiser et al., 2008). However, live-cell imaging showed that CBs are highly mobile (Platani et al., 2000, 2002) and preformed CBs are recruited to active snRNA genes, suggesting that CBs do not

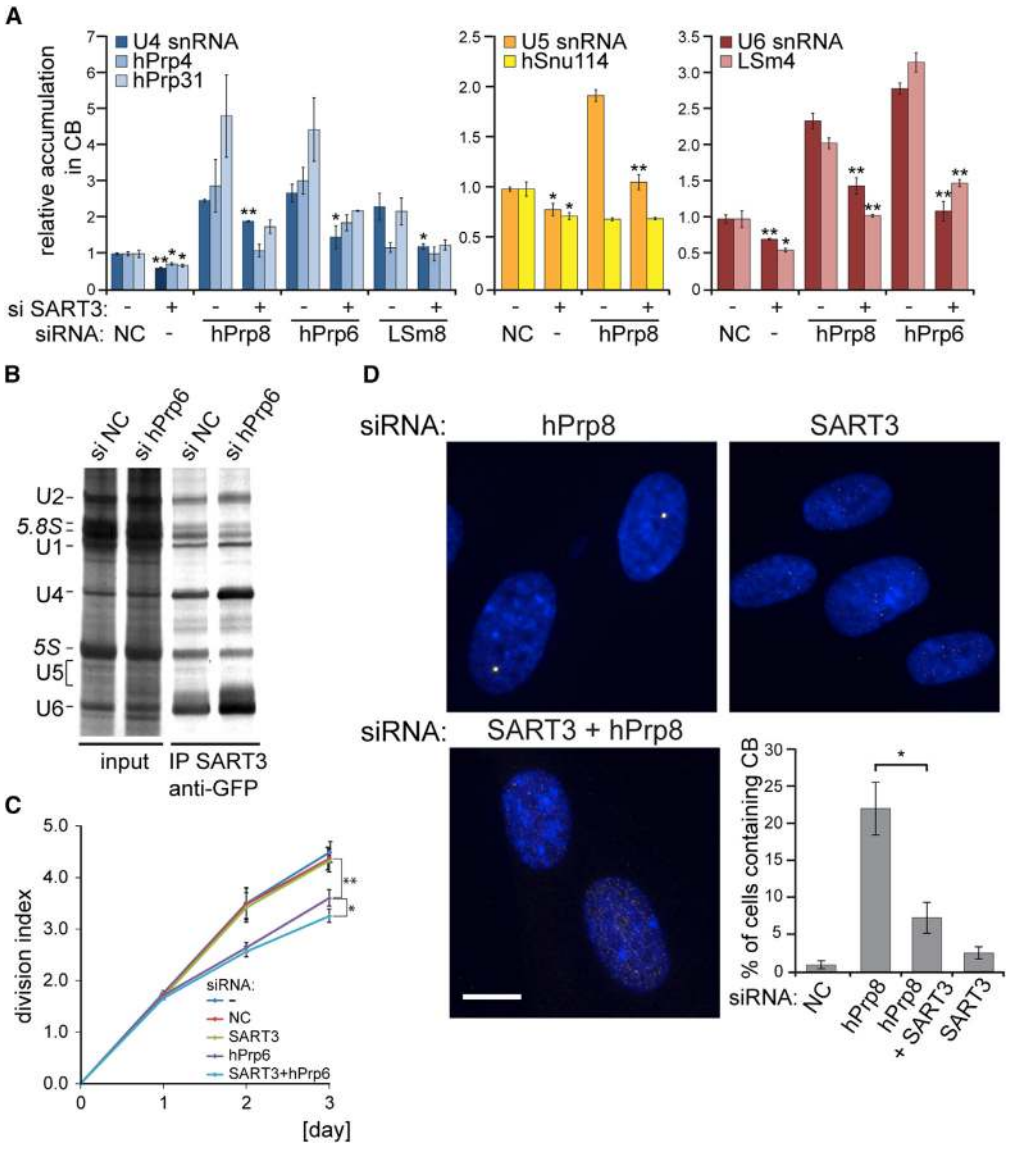

Figure 7. SART3 Bridges Tri-snRNP Components to Cajal Bodies

(A) Cells were treated with siRNA against SART3 alone or in combination with siRNAs against hPrp8, hPrp6, or LSm8 and CB localization of individual snRNPs measured by high-content microscopy. The average of three experiments is shown together with the SEM. *p ≤ 0.05, **p ≤ 0.01 of t test against noncoding. See also Figures S2–S4 for microscopy images.

(B) Increased interaction of SART3 with U4 and U6 snRNAs after inhibition of tri-snRNP assembly by hPrp6 knockdown. SART3-GFP was immunoprecipitated and coprecipitated snRNAs detected on gel by silver staining.

(C) Depletion of SART3 enhances proliferation defects caused by hPrp6 depletion while single SART3 knockdown does not influence cell division. The average of three experiments is shown together with the SEM. *p ≤ 0.05, **p ≤ 0.01 of t test.

(D) Formation of new CBs in primary fibroblasts WI-38 induced by hPrp8 downregulation is reduced after SART3 knockdown. The average of three experiments is shown together with the SEM. *p ≤ 0.05 of t test.

primarily form around a specific gene locus (Dundr et al., 2007). CBs are induced upon overexpression of snRNP-specific Sm proteins (Sleeman et al., 2001), which indicates that CB formation depends on the concentration of snRNP components. Here, we suggest if snRNP disassembly and recycling are in balance, the amount of snRNP assembly intermediates is low and CBs do not form. Our data are consistent with this hypothesis and show that inhibition of tri-snRNP assembly triggers CB formation in primary fibroblasts, which normally lack visible CBs. We propose that a higher concentration of incomplete snRNPs together with SART3 can, directly or indirectly, induce coilin oligomerization, which leads to nucleation of microscopically visible CBs. Recently, an RNA-dependent aggregation of plant coilin was observed in vitro (Makarov et al., 2013). Human and frog

coilin also interact with nucleic acids (Bellini and Gall, 1998; Broome and Hebert, 2013; Machyna et al., 2014), but the effect of RNA on animal coilin multimerization is unknown.

The presented model for CB nucleation implies that there are at least two essential components—coilin and incomplete snRNPs. Only when the concentration of both components reaches a critical value they nucleate large structures—CBs. The concentration of coilin in primary fibroblast is apparently high enough to support CB formation, and thus increasing concentration of the second component—incomplete snRNPs—induces CBs. The depletion of the bridging factor SART3, which reduced formation of CBs in fibroblasts, further shows the importance of the snRNP—coilin association for CB formation (Figure 7D). This two-component hypothesis also explains why overexpression of just one component—coilin—does not trigger CB assembly (Sleeman et al., 2001). These findings suggest that CB appearance is caused by an imbalance in the snRNP assembly/recycling pathway, which can occur in highly metabolically active cells where CBs are often present. Increasing the transcription/splicing level (e.g., in embryonic cells or cancer cells) leads to higher rates of mono-snRNP production and creates an imbalance in snRNP recycling, triggering the formation of CBs to buffer incomplete intermediates. Indeed, normal CBs found in HeLa cells contain a high concentration of SART3-U4/U6 snRNP complexes, suggesting that this assembly intermediate is present in HeLa cells under normal conditions and is preferentially localized in CBs (Staněk and Neugebauer, 2004).

Taken together, our data point to a surveillance pathway that controls the final steps of snRNP formation and sequesters incomplete snRNPs in CBs. Segregation of stalled assembly intermediates in CBs provides cells with a buffering system that helps to maintain snRNP homeostasis in the nucleoplasm.

EXPERIMENTAL PROCEDURES

Cells and Antibodies

HeLa cells, stable cell lines derived from HeLa cells, and human primary fibroblasts WI38 were cultured in Dulbecco's modified Eagle's medium (DMEM) supplemented with 10% fetal calf serum (FCS), penicillin, and streptomycin (Invitrogen). HeLa cells stably expressing SART3-GFP, hPrp4-GFP, hPrp8-GFP, hPrp31-GFP, and LSm4-GFP from bacterial artificial chromosome were prepared as described previously (Poser et al., 2008) and kindly provided by Ina Poser and Tony Hyman (MPI-CBG, Dresden, Germany). SART3-GFP constructs were described previously (Staněk et al., 2003).

For western blotting, we used primary antibodies: rabbit anti-hPrp8 (H-300, Santa Cruz Biotechnology), anti-hPrp6 (H-300; Santa Cruz Biotechnology), rabbit anti-SART3 (Staněk et al., 2003), rabbit anti-hBrr2 (Sigma-Aldrich), mouse anti-LSm8 (sc-81315; Santa Cruz Biotechnology), mouse anti-tubulin (provided by P. Dráber, IMG AS CR, Prague, Czech Republic) (Dráber et al., 1989), and mouse anti-GAPDH (9484, Abcam). Secondary goat antibodies anti-mouse or anti-rabbit conjugated with horseradish peroxidase (Jackson ImmunoResearch Laboratories) were utilized. For indirect immunostaining, we used the primary rabbit antibodies anti-SART3/p110 (Staněk et al., 2003), anti-LSm4 (Achsel et al., 1999), anti-hPrp31 (Makarova et al., 2002), anti-hPrp4 (Lauber et al., 1997), and anti-hSnu114 (Fabrizio et al., 1997). Antibodies against LSm4, hPrp4, hPrp31, and hSnu114 were kindly provided by R. Lührmann (Max Planck Institute). The monoclonal antibody against U2B′′ was purchased from Progen. The anti-coilin (5P10) mouse antibody, provided by M. Carmo-Fonseca (Institute of Molecular Medicine, Lisbon, Portugal) (Almeida et al., 1998), or anti-coilin (H-300, Santa Cruz Biotechnology) were used to mark CBs. Secondary anti-mouse or anti-rabbit goat antibodies were conjugated with DyLight488, DyLight549, or Cy5 (Jackson ImmunoResearch Laboratories). For immunoprecipitation, we used mouse anti-Sm (Y12) produced by the facility of IMG ASCR or goat anti-GFP obtained from David Drechsel, MPI-CBG, Dresden, Germany.

RNAi

The siRNA used in this study was SART3 (5′-ACUGCUACGUGGAGUUUAAtt-3′; the sequence was kindly provided by Konstantin Licht (Institute of Biochemistry, Justus-Liebig-University of Giessen, Germany). Additional anti-SART3 siRNAs tested were SART3-2 (5′-GCUGUUUCUGAGAAAGUG Att-3′) and SART3-3 (5′-AAGUGUCAUACAAAAAGGGtt-3′). hPrp8 (5′-CCUGU AUGCCUGACCGUUUtt-3′) is designed against the sequence around the STOP codon and does not target hPrp8-GFP used for rescue experiments. siRNA against LSm8 was published in (Novotny et al., 2012) and against hPrp6 in (Schaffert et al., 2004). Two additional siRNAs tested against LSm8 were 5′-AAGUGGUACUAGGAUUAUAtt-3′ and 5′-CAUCAGAUGGGAGAAU GAUtt-3′ and against hPrp6 5′-CCCUCGAGCAUGUUCCAAAtt-3 and 5′-GAUAAAAGGAUGGAUGAAAtt-3′.

Preannealed siRNA duplexes were obtained from Ambion (Applied Biosystems). The "negative control 1" siRNA from Ambion was used as a negative control. All siRNAs were transfected using Oligofectamine (Invitrogen) according to the manufacturer's protocol, and cells were cultured for additional 48 hr (HeLa) or 72 hr (WI38). See Figure S6A for knockdown efficiencies.

RT-PCR

Total RNA was isolated 48 hr after siRNA transfection by using TRIzol reagent (Invitrogen) according to the manufacturer's protocol, and cDNA was synthesized using random hexamers (Eastport) by SuperScript III (Invitrogen). Quantitative PCR was done as previously described (Listerman et al., 2006). snRNA levels were calculated according to $R = 2^{\Delta C_{(c_{NCsiRNA} - c_{spec.siRNA})}}$ and normalized to 18S rRNA.

Immunofluorescence and Image Acquisition

Cells were fixed and labeled as previously described (Novotný et al., 2011). snRNAs were visualized by fluorescent in situ hybridization as previously described (Stanek et al., 2008). Images were acquired using the DeltaVision microscopic system (Applied Precision) coupled to the Olympus IX70 microscope equipped with an oil-immersion objective (60×/1.4 numerical aperture [NA]) and restored using a measured point spread function (SoftWorx; Applied Precision) as previously described (Novotný et al., 2011).

For high-content microscopy, samples were scanned using automated acquisition driven by the Acquisition Scan^R program using Scan^R system (Olympus) equipped with an oil-immersion objective (60×/1.35 NA). A total of 225 images were taken per sample. Several hundreds of cells were collected per sample. Each image was reconstructed from stacks of ten optical sections with 300 nm z step and automatically restored using a measured point spread function implemented in the Analysis Scan^R software (Olympus). Cellular compartments were automatically identified based on fluorescence intensity combined with compartment edge detection. Cell nuclei were visualized using 4′,6-diamidino-2-phenylindole (DAPI) staining, and anti-coilin antibody was used to visualize CBs. Total intensities, areas, and counts for each cellular object were obtained using the Analysis Scan^R software. The ratio of fluorescence in CBs versus the nucleoplasm was calculated according to

$$R = \frac{\frac{\sum total\ IF_{CB\ per\ nucleus}}{\sum Area_{CB\ per\ nucleus}}}{\frac{total\ IF_{nucleus} - \sum total\ IF_{CB\ per\ nucleus}}{Area_{nucleus} - \sum Area_{CB\ per\ nucleus}}},$$

where the mean of CB intensities per nucleus was calculated and then divided by the mean fluorescence of the rest of the nucleus. The mean and SEM of three biological experiments were calculated and plotted.

For structured-illumination microscopy, acquisition was performed on the Delta Vision OMX (Applied Precision) imaging system equipped with 3D structured illumination (3D-SIM) and a 60×/1.42 NA objective, and 0.125 μm optical sections were acquired. For the image reconstruction, we used the SoftWorx

(Applied Precision) software implemented with the 3D SI Reconstruction function.

RNA Synthesis and Microinjection

U4 snRNA (full-length or mutant lacking U6-base-pairing domain) was prepared as described previously (Klingauf et al., 2006) by in vitro transcription kit (MEGAshortScript kit, Ambion) in the presence of UTP-Alexa 488 and the cap analog (m^7G(5′)ppp(5′)G) (Life Technologies). RNA was diluted in nuclease free water with dextran-TRITC 70 kDa (Sigma-Aldrich) to a final concentration of 150 ng/μl. snRNAs were microinjected into HeLa cells using micromanipulator (Narishige) coupled with Eppendorf Microjet using Femtotips II (Eppendorf). Cells were incubated for a given time period and fixed, and coilin was detected by indirect immunofluorescence. The average of 40–80 CBs (15–25 cells) is shown together with SEM.

snRNP Immunoprecipitation and Western Blot Analysis

Cells were grown on a 15 cm Petri dish for 28 hr. Immunoprecipitation was performed as previously described (Huranová et al., 2009) using mouse anti-Sm or goat anti–GFP antibodies. RNA was extracted using phenol/chloroform, resolved on a 7 M urea denaturing polyacrylamide gel and silver stained. For protein analysis, cells were directly lysed in SDS-sample buffer. Proteins were resolved on an SDS-PAGE gel and detected by western blotting.

Yeast Two-Hybrid Assay

Coilin cDNA was obtained from HeLa cell total RNA by RT-PCR and inserted into pGADT7 (Clontech) using the restriction sites SfiI and SmaI. ΔRRMΔCT and ΔEΔRRMΔCT were cloned into pGBKT7 using the restriction sites EcoRI and SalI. Two-hybrid experiments were performed with the *S. cerevisiae* strain AH109 (Matchmaker, Clontech), which was cotransformed by the lithium acetate procedure using pGADT7 and pGBKT7-derived vectors. Transformed cells were selected on minimal medium containing adenine and essential amino acids except tryptophan and leucine. For interaction tests, five colonies from each cotransformant were transferred to selection minimal medium lacking both adenine and histidine.

Proliferation Assay

HeLa cells were trypsinized, collected at 500 × *g*, and resuspended to a concentration of 2 × 10^7 cells/ml in PBS buffer. Carboxyfluorescein diacetate succinimidyl ester (CFSE) was added to 1.5 μM final concentration. Cells were incubated for 10 min at 37°C and residual extracellular staining was quenched by adding 10 ml of ice-cold DMEM plus 10% FSC and incubated on ice for 5 min. Cells were washed 3x in the medium (DMEM + 10% FCS), collected at 500 × *g* and resuspended in DMEM + 10% FCS. The fluorescence of cells was measured by BD LSR II flow cytometer (BD Biosciences) using a 488 nm laser and results were calculated using the flow cytometry analysis software FlowJo 7.6 (Tree Star). The siRNA transfection was performed 24 hr after CFSE staining and cells measured every 24 hr for the next 3 days.

SUPPLEMENTAL INFORMATION

Supplemental Information includes six figures and can be found with this article online at http://dx.doi.org/10.1016/j.celrep.2014.12.030.

AUTHOR CONTRIBUTIONS

I.N. and D.S. conceived of the overall study. I.N. knocked down hPrp6, LSm8, and SART3; localized and quantified snRNP localization in CBs; performed immunoprecipitation, RNA gels, and western blotting; and analyzed cell viability. A.M. performed the rescue experiment with hPrp8-GFP. E.S. quantified CB localization of hPrp31-GFP and significantly contributed to manuscript writing and figure organization. D.M. performed hPrp8 knockdown and localization of snRNAs. K.K. immunoprecipitated SART3-GFP constructs followed by snRNA and protein detection. A.R. microinjected U4 snRNAs and quantified their CB accumulation. M.S. and Z.K. performed the yeast two-hybrid assay. The first draft of the manuscript was written by I.N. and rewritten by D.S.

ACKNOWLEDGMENTS

We are grateful to Karla Neugebauer, Reinhard Lührmann, Pavel Dráber, Maria Carmo-Fonseca, and David Drechsel for providing us with antibodies, Ina Poser and Tony Hyman for BAC cell lines expressing GFP-tagged proteins, and Ondřej Horváth for help with the proliferation assay. We thank Jan Peychl from MPI-CBG in Dresden and Euro-BioImaging initiative for support of super-resolution microscopy. We also thank Karla Neugebauer and members of the Staněk lab for useful comments on the manuscript and Kimberly Kotovic for language proofreading. This work was supported by the Czech Science Foundation (P302/11/1910 to D.S. and P302/12/1895 to Z.K.), the Czech Ministry of Education, Youth and Sports (LH14033 to D.S.), and the Academy of Sciences of the Czech Republic (RVO68378050 and M200521206 to D.S.).

Received: June 2, 2014
Revised: September 18, 2014
Accepted: December 13, 2014
Published: January 15, 2015

REFERENCES

Achsel, T., Brahms, H., Kastner, B., Bachi, A., Wilm, M., and Lührmann, R. (1999). A doughnut-shaped heteromer of human Sm-like proteins binds to the 3′-end of U6 snRNA, thereby facilitating U4/U6 duplex formation in vitro. EMBO J. *18*, 5789–5802.

Almeida, F., Saffrich, R., Ansorge, W., and Carmo-Fonseca, M. (1998). Microinjection of anti-coilin antibodies affects the structure of coiled bodies. J. Cell Biol. *142*, 899–912.

Battle, D.J., Kasim, M., Yong, J., Lotti, F., Lau, C.K., Mouaikel, J., Zhang, Z., Han, K., Wan, L., and Dreyfuss, G. (2006). The SMN complex: an assembly machine for RNPs. Cold Spring Harb. Symp. Quant. Biol. *71*, 313–320.

Bell, M., Schreiner, S., Damianov, A., Reddy, R., and Bindereif, A. (2002). p110, a novel human U6 snRNP protein and U4/U6 snRNP recycling factor. EMBO J. *21*, 2724–2735.

Bellini, M., and Gall, J.G. (1998). Coilin can form a complex with the U7 small nuclear ribonucleoprotein. Mol. Biol. Cell *9*, 2987–3001.

Boon, K.L., Grainger, R.J., Ehsani, P., Barrass, J.D., Auchynnikava, T., Inglehearn, C.F., and Beggs, J.D. (2007). prp8 mutations that cause human retinitis pigmentosa lead to a U5 snRNP maturation defect in yeast. Nat. Struct. Mol. Biol. *14*, 1077–1083.

Boulisfane, N., Choleza, M., Rage, F., Neel, H., Soret, J., and Bordonné, R. (2011). Impaired minor tri-snRNP assembly generates differential splicing defects of U12-type introns in lymphoblasts derived from a type I SMA patient. Hum. Mol. Genet. *20*, 641–648.

Broome, H.J., and Hebert, M.D. (2013). Coilin displays differential affinity for specific RNAs in vivo and is linked to telomerase RNA biogenesis. J. Mol. Biol. *425*, 713–724.

Chari, A., Paknia, E., and Fischer, U. (2009). The role of RNP biogenesis in spinal muscular atrophy. Curr. Opin. Cell Biol. *21*, 387–393.

Collier, S., Pendle, A., Boudonck, K., van Rij, T., Dolan, L., and Shaw, P. (2006). A distant coilin homologue is required for the formation of cajal bodies in Arabidopsis. Mol. Biol. Cell *17*, 2942–2951.

Darzacq, X., Jády, B.E., Verheggen, C., Kiss, A.M., Bertrand, E., and Kiss, T. (2002). Cajal body-specific small nuclear RNAs: a novel class of 2′-O-methylation and pseudouridylation guide RNAs. EMBO J. *21*, 2746–2756.

Dráber, P., Dráberová, E., Linhartová, I., and Viklický, V. (1989). Differences in the exposure of C- and N-terminal tubulin domains in cytoplasmic microtubules detected with domain-specific monoclonal antibodies. J. Cell Sci. *92*, 519–528.

Dundr, M., Ospina, J.K., Sung, M.H., John, S., Upender, M., Ried, T., Hager, G.L., and Matera, A.G. (2007). Actin-dependent intranuclear repositioning of an active gene locus in vivo. J. Cell Biol. *179*, 1095–1103.

Fabrizio, P., Laggerbauer, B., Lauber, J., Lane, W.S., and Lührmann, R. (1997). An evolutionarily conserved U5 snRNP-specific protein is a GTP-binding factor closely related to the ribosomal translocase EF-2. EMBO J. *16*, 4092–4106.

Ferreira, J.A., Carmo-Fonseca, M., and Lamond, A.I. (1994). Differential interaction of splicing snRNPs with coiled bodies and interchromatin granules during mitosis and assembly of daughter cell nuclei. J. Cell Biol. *126*, 11–23.

Frey, M.R., and Matera, A.G. (1995). Coiled bodies contain U7 small nuclear RNA and associate with specific DNA sequences in interphase human cells. Proc. Natl. Acad. Sci. USA *92*, 5915–5919.

Frey, M.R., Bailey, A.D., Weiner, A.M., and Matera, A.G. (1999). Association of snRNA genes with coiled bodies is mediated by nascent snRNA transcripts. Curr. Biol. *9*, 126–135.

Huranová, M., Hnilicová, J., Fleischer, B., Cvacková, Z., and Stanek, D. (2009). A mutation linked to retinitis pigmentosa in HPRP31 causes protein instability and impairs its interactions with spliceosomal snRNPs. Hum. Mol. Genet. *18*, 2014–2023.

Huranová, M., Ivani, I., Benda, A., Poser, I., Brody, Y., Hof, M., Shav-Tal, Y., Neugebauer, K.M., and Stanek, D. (2010). The differential interaction of snRNPs with pre-mRNA reveals splicing kinetics in living cells. J. Cell Biol. *191*, 75–86.

Jacobs, E.Y., Frey, M.R., Wu, W., Ingledue, T.C., Gebuhr, T.C., Gao, L., Marzluff, W.F., and Matera, A.G. (1999). Coiled bodies preferentially associate with U4, U11, and U12 small nuclear RNA genes in interphase HeLa cells but not with U6 and U7 genes. Mol. Biol. Cell *10*, 1653–1663.

Jády, B.E., Darzacq, X., Tucker, K.E., Matera, A.G., Bertrand, E., and Kiss, T. (2003). Modification of Sm small nuclear RNAs occurs in the nucleoplasmic Cajal body following import from the cytoplasm. EMBO J. *22*, 1878–1888.

Kaiser, T.E., Intine, R.V., and Dundr, M. (2008). De novo formation of a subnuclear body. Science *322*, 1713–1717.

Klingauf, M., Stanek, D., and Neugebauer, K.M. (2006). Enhancement of U4/U6 small nuclear ribonucleoprotein particle association in Cajal bodies predicted by mathematical modeling. Mol. Biol. Cell *17*, 4972–4981.

Lauber, J., Plessel, G., Prehn, S., Will, C.L., Fabrizio, P., Gröning, K., Lane, W.S., and Lührmann, R. (1997). The human U4/U6 snRNP contains 60 and 90kD proteins that are structurally homologous to the yeast splicing factors Prp4p and Prp3p. RNA *3*, 926–941.

Lemm, I., Girard, C., Kuhn, A.N., Watkins, N.J., Schneider, M., Bordonné, R., and Lührmann, R. (2006). Ongoing U snRNP biogenesis is required for the integrity of Cajal bodies. Mol. Biol. Cell *17*, 3221–3231.

Listerman, I., Sapra, A.K., and Neugebauer, K.M. (2006). Cotranscriptional coupling of splicing factor recruitment and precursor messenger RNA splicing in mammalian cells. Nat. Struct. Mol. Biol. *13*, 815–822.

Liu, J.L., Wu, Z., Nizami, Z., Deryusheva, S., Rajendra, T.K., Beumer, K.J., Gao, H., Matera, A.G., Carroll, D., and Gall, J.G. (2009). Coilin is essential for Cajal body organization in Drosophila melanogaster. Mol. Biol. Cell *20*, 1661–1670.

Machyna, M., Heyn, P., and Neugebauer, K.M. (2013). Cajal bodies: where form meets function. Wiley Interdiscip. Rev. RNA *4*, 17–34.

Machyna, M., Kehr, S., Straube, K., Kappei, D., Buchholz, F., Butter, F., Ule, J., Hertel, J., Stadler, P., and Neugebauer, K.M. (2014). Global identification of coilin binding partners reveals hundreds of small non-coding RNAs that traffic through Cajal bodies. Mol. Cell *56*, 389–399.

Makarov, E.M., Makarova, O.V., Achsel, T., and Lührmann, R. (2000). The human homologue of the yeast splicing factor prp6p contains multiple TPR elements and is stably associated with the U5 snRNP via protein-protein interactions. J. Mol. Biol. *298*, 567–575.

Makarov, V., Rakitina, D., Protopopova, A., Yaminsky, I., Arutiunian, A., Love, A.J., Taliansky, M., and Kalinina, N. (2013). Plant coilin: structural characteristics and RNA-binding properties. PLoS ONE *8*, e53571.

Makarova, O.V., Makarov, E.M., Liu, S., Vornlocher, H.P., and Lührmann, R. (2002). Protein 61K, encoded by a gene (PRPF31) linked to autosomal dominant retinitis pigmentosa, is required for U4/U6*U5 tri-snRNP formation and pre-mRNA splicing. EMBO J. *21*, 1148–1157.

Marshallsay, C., and Lührmann, R. (1994). In vitro nuclear import of snRNPs: cytosolic factors mediate m3G-cap dependence of U1 and U2 snRNP transport. EMBO J. *13*, 222–231.

Matera, A.G., and Shpargel, K.B. (2006). Pumping RNA: nuclear bodybuilding along the RNP pipeline. Curr. Opin. Cell Biol. *18*, 317–324.

Matera, A.G., and Wang, Z. (2014). A day in the life of the spliceosome. Nat. Rev. Mol. Cell Biol. *15*, 108–121.

Medenbach, J., Schreiner, S., Liu, S., Lührmann, R., and Bindereif, A. (2004). Human U4/U6 snRNP recycling factor p110: mutational analysis reveals the function of the tetratricopeptide repeat domain in recycling. Mol. Cell. Biol. *24*, 7392–7401.

Morris, G.E. (2008). The Cajal body. Biochim. Biophys. Acta *1783*, 2108–2115.

Narayanan, U., Achsel, T., Lührmann, R., and Matera, A.G. (2004). Coupled in vitro import of U snRNPs and SMN, the spinal muscular atrophy protein. Mol. Cell *16*, 223–234.

Nesic, D., Tanackovic, G., and Krämer, A. (2004). A role for Cajal bodies in the final steps of U2 snRNP biogenesis. J. Cell Sci. *117*, 4423–4433.

Nizami, Z., Deryusheva, S., and Gall, J.G. (2010). The Cajal body and histone locus body. Cold Spring Harb. Perspect. Biol. *2*, a000653.

Nottrott, S., Urlaub, H., and Lührmann, R. (2002). Hierarchical, clustered protein interactions with U4/U6 snRNA: a biochemical role for U4/U6 proteins. EMBO J. *21*, 5527–5538.

Novotný, I., Blažíková, M., Staněk, D., Herman, P., and Malinsky, J. (2011). In vivo kinetics of U4/U6·U5 tri-snRNP formation in Cajal bodies. Mol. Biol. Cell *22*, 513–523.

Novotny, I., Podolská, K., Blazíková, M., Valásek, L.S., Svoboda, P., and Stanek, D. (2012). Nuclear LSm8 affects number of cytoplasmic processing bodies via controlling cellular distribution of Like-Sm proteins. Mol. Biol. Cell *23*, 3776–3785.

Ospina, J.K., Gonsalvez, G.B., Bednenko, J., Darzynkiewicz, E., Gerace, L., and Matera, A.G. (2005). Cross-talk between snurportin1 subdomains. Mol. Biol. Cell *16*, 4660–4671.

Patel, S.B., and Bellini, M. (2008). The assembly of a spliceosomal small nuclear ribonucleoprotein particle. Nucleic Acids Res. *36*, 6482–6493.

Platani, M., Goldberg, I., Swedlow, J.R., and Lamond, A.I. (2000). In vivo analysis of Cajal body movement, separation, and joining in live human cells. J. Cell Biol. *151*, 1561–1574.

Platani, M., Goldberg, I., Lamond, A.I., and Swedlow, J.R. (2002). Cajal body dynamics and association with chromatin are ATP-dependent. Nat. Cell Biol. *4*, 502–508.

Poser, I., Sarov, M., Hutchins, J.R., Hériché, J.K., Toyoda, Y., Pozniakovsky, A., Weigl, D., Nitzsche, A., Hegemann, B., Bird, A.W., et al. (2008). BAC TransgeneOmics: a high-throughput method for exploration of protein function in mammals. Nat. Methods *5*, 409–415.

Rader, S.D., and Guthrie, C. (2002). A conserved Lsm-interaction motif in Prp24 required for efficient U4/U6 di-snRNP formation. RNA *8*, 1378–1392.

Schaffert, N., Hossbach, M., Heintzmann, R., Achsel, T., and Lührmann, R. (2004). RNAi knockdown of hPrp31 leads to an accumulation of U4/U6 di-snRNPs in Cajal bodies. EMBO J. *23*, 3000–3009.

Shpargel, K.B., and Matera, A.G. (2005). Gemin proteins are required for efficient assembly of Sm-class ribonucleoproteins. Proc. Natl. Acad. Sci. USA *102*, 17372–17377.

Sleeman, J.E., and Lamond, A.I. (1999). Newly assembled snRNPs associate with coiled bodies before speckles, suggesting a nuclear snRNP maturation pathway. Curr. Biol. *9*, 1065–1074.

Sleeman, J.E., Ajuh, P., and Lamond, A.I. (2001). snRNP protein expression enhances the formation of Cajal bodies containing p80-coilin and SMN. J. Cell Sci. *114*, 4407–4419.

Smith, K.P., Carter, K.C., Johnson, C.V., and Lawrence, J.B. (1995). U2 and U1 snRNA gene loci associate with coiled bodies. J. Cell. Biochem. *59*, 473–485.

Staněk, D., and Neugebauer, K.M. (2004). Detection of snRNP assembly intermediates in Cajal bodies by fluorescence resonance energy transfer. J. Cell Biol. *166*, 1015–1025.

Stanek, D., and Neugebauer, K.M. (2006). The Cajal body: a meeting place for spliceosomal snRNPs in the nuclear maze. Chromosoma *115*, 343–354.

Staněk, D., Rader, S.D., Klingauf, M., and Neugebauer, K.M. (2003). Targeting of U4/U6 small nuclear RNP assembly factor SART3/p110 to Cajal bodies. J. Cell Biol. *160*, 505–516.

Stanek, D., Pridalova-Hnilicova, J., Novotny, I., Huranova, M., Blazikova, M., Wen, X., Sapra, A.K., and Neugebauer, K.M. (2008). Spliceosomal small nuclear ribonucleoprotein particles repeatedly cycle through Cajal bodies. Mol Biol Cell *19*, 2534–2543.

Strzelecka, M., Oates, A.C., and Neugebauer, K.M. (2010a). Dynamic control of Cajal body number during zebrafish embryogenesis. Nucleus *1*, 96–108.

Strzelecka, M., Trowitzsch, S., Weber, G., Lührmann, R., Oates, A.C., and Neugebauer, K.M. (2010b). Coilin-dependent snRNP assembly is essential for zebrafish embryogenesis. Nat. Struct. Mol. Biol. *17*, 403–409.

Suzuki, T., Izumi, H., and Ohno, M. (2010). Cajal body surveillance of U snRNA export complex assembly. J. Cell Biol. *190*, 603–612.

Tucker, K.E., Berciano, M.T., Jacobs, E.Y., LePage, D.F., Shpargel, K.B., Rossire, J.J., Chan, E.K., Lafarga, M., Conlon, R.A., and Matera, A.G. (2001). Residual Cajal bodies in coilin knockout mice fail to recruit Sm snRNPs and SMN, the spinal muscular atrophy gene product. J. Cell Biol. *154*, 293–307.

Walker, M.P., Tian, L., and Matera, A.G. (2009). Reduced viability, fertility and fecundity in mice lacking the cajal body marker protein, coilin. PLoS ONE *4*, e6171.

Whittom, A.A., Xu, H., and Hebert, M.D. (2008). Coilin levels and modifications influence artificial reporter splicing. Cell. Mol. Life Sci. *65*, 1256–1271.